Rapid Communication

An improved two-dimensional unstructured CE/SE scheme for capturing shock waves*

Fu Zheng(付 峥)[a] and Liu Kai-Xin(刘凯欣)[a)b)†]

[a] *LTCS and Department of Mechanics and Aerospace Engineering, College of Engineering, Peking University, Beijing* 100871 *China*

[b] *Center for Applied Physics and Technology, Peking University, Beijing* 100871, *China*

(Received 11 November 2011; revised manuscript received 19 December 2011)

In this paper, the accuracy of Chang's unstructured space–time conservation element and solution element (CE/SE) scheme is analysed for the first time. Based on a redefinition of conservation elements and solution elements, an improved two-dimensional (2D) unstructured CE/SE scheme with an adjustable parameter β is proposed to accurately capture shock waves. The new scheme can be applied to any type of grid without special treatment. Compared with Chang's original parameter α, larger β dose not cost extra computational resources. Numerical tests reveal that the new scheme is not only clear in physical concept, compact and highly accurate but also more capable of capturing shock waves than the popular fifth-order accurate weighted essentially non-oscillatory scheme.

Keywords: CE/SE method, unstructured mesh, high-order accurate scheme, shock waves

PACS: 02.60.Cb, 47.40.–x **DOI:** 10.1088/1674-1056/21/4/040202

1. Introduction

The accurate and efficient simulation of shock waves plays an important role in the numerical simulation of various physics problems ranging from detonation, nuclear explosion to spall fracture. For example, in aeronautics, shock waves around a travelling supersonic or hypersonic vehicle often lead to highly localized temperature and high heating rate on the surface of the vehicle. The vehicle may be severely damaged at such a high temperature and heating rate. In order to obtain accurate shock waves, high-order methods[1,2] have been developed. However, numerical tests indicate that total variation diminishing (TVD) classical essentially non-oscillatory (ENO) or weighted ENO (WENO) schemes may lead to a significant damping of the acoustic fluctuations.[3] The reconstruction procedure of ENO or WENO schemes is also difficult and expensive for multidimensional unstructured simulations.[4] Moreover, the Courant number severely decreases for high-order accurate schemes. If the accuracy is higher than the fourth order, the Runge–Kutta (RK) method, which is widely used for discretizing time, becomes too expensive to be carried out.[4] Therefore, new schemes, such as the space–time conservation element and the solution element method (CE/SE),[5] have been proposed.

The CE/SE method[5] is an explicit, accurate, and efficient scheme for solving conservation laws. It is substantially different in both concept and methodology from traditional methods. By treating space and time uniformly and introducing the concepts of conservation element (CE) and solution element (SE), the conservation laws are enforced locally and globally in both time and space. The spatial derivatives are also stored and calculated. In this way, the CE/SE method is compact and highly accurate. In order to capture sharp shocks, the basic scheme[5] of the CE/SE method is non-dissipative and several weighted averaging techniques[6] are developed.

During the past two decades, the CE/SE method became successful in several fields such as MHD,[7,8] detonation,[9−15] and spall fracture.[16] Chang's original CE/SE scheme is based on triangular or tetrahedral grids. The range of courant number is between 0.1 and 1. Now, besides triangular and tetrahedral grids, it can also calculate on quadrangular and hexahedral grids.[17,18] The courant number range is expanded roughly from 0.0001 to 1, due to the courant number insensitive CE/SE (CNI-CE/SE) scheme.[19] Recently, several high-order schemes[6] have been proposed. All the above CE/SE schemes are based on Chang's defi-

*Project supported by the National Natural Science Foundation of China (Grant Nos. 10732010 and 10972010).

†Corresponding author. E-mail: kliu@pku.edu.cn

© 2012 Chinese Physical Society and IOP Publishing Ltd

nition of CE and SE. To simplify the CE/SE method while calculating at structured grids, an improved CE/SE method and its high-order accurate scheme, which is based on a redefinition of smaller CE and SE, are proposed and investigated.[8−14,16,20,21] Their scheme has smaller spatial steps. The derivatives are calculated based on two groups of equations instead of Chang's four groups.

Despite the inconvenience of simulation on structured grids, unstructured CE/SE schemes show great potential for large scale engineering simulations. The generation of structured grids for complex geometry costs much more time and it is more complicated. Unstructured grids are much simpler to deal with boundary conditions and they are more flexible for adaptive simulation. Unlike traditional CFD methods, the accuracy of the CE/SE scheme is based on the order of derivatives stored at the computational node. This retains the compact feature which is suitable for large scale parallel simulation.

Nevertheless, Chang's definitions of CE and SE need special treatment[22] while calculating on unstructured grids. This complicates the construction procedure and reduces the accuracy of the CE/SE method. The dissipation due to the parameter α is also restricted between the minmod function and the average of all derivative terms at neighbouring centroids. The computational resource is also significantly increased to obtain stronger dissipation. Numerical examples indicate that only $\alpha \leq 128$ is acceptable for most computers. Furthermore, most of the numerical characteristics of Chang's scheme are inherited by the other unstructured CE/SE schemes including the CNI-CE/SE scheme. Hence, theoretical and numerical investigations of Chang's scheme are of fundamental importance to develop novel CE/SE scheme and to predict the numerical behaviour of the existing CE/SE scheme. Unfortunately, the numerical characteristic of Chang's unstructured scheme has never been theoretically investigated due to complexity and difficulty.

In this paper, the accuracy of Chang's unstructured CE/SE scheme is first analysed. Then redefinitions of CE and SE are proposed. In order to improve the accuracy of the new scheme and increase the range of dissipation, an extra parameter β is also introduced. Moreover, the accuracy and the efficiency of the new scheme are investigated in detail through two numerical examples.

2. Analysis of Chang's CE/SE scheme

Consider the following 2D Euler equation:

$$\frac{\partial \boldsymbol{U}}{\partial t} + \frac{\partial \boldsymbol{E}}{\partial x} + \frac{\partial \boldsymbol{F}}{\partial y} = 0, \tag{1}$$

where $\boldsymbol{U}$ are the vector of variable, $\boldsymbol{E}$ and $\boldsymbol{F}$ are two functions of $\boldsymbol{U}$. Let $x_1 = x$, $x_2 = y$, and $x_3 = t$ be the coordinates of a Euclidean space E_3. By using the divergence theorem in E_3, equation (1) is equivalent to the integral equation

$$\oint_{S(V)} \boldsymbol{h}_m \cdot \mathrm{d}\boldsymbol{S} = 0, \ (m = 1, 2, \ldots, M_{\mathrm{eqs}}), \tag{2}$$

where M_{eqs}, $S(V)$, $\mathrm{d}\boldsymbol{S}$, and $\boldsymbol{h}_m$ denote the number of equations, the boundary of an arbitrary space–time region V in E_3, the surface vector of V, and the vector (E_m, F_m, U_m), respectively

In Fig. 1(a), point G, marked by $\bullet$, is the centroid of ΔBDF. A, C, and E, marked by $\circ$, are the centroids of ΔFMB, ΔBJD, and ΔDLF, respectively. Point $\bar{G}$, marked by $\blacksquare$, is the centroid of hexagon $ABCDEF$, and it is also the solution point of ΔBDF. Points $\bar{A}$, $\bar{C}$, and $\bar{E}$, marked by $\square$, are the solution points of ΔFMB, ΔBJD, and ΔDLF, respectively. In the space–time domain, points without any superscript are at the time level t_n, and points with superscript $'$ and $''$ as shown in Fig. 1(b), are at the time level $t_n + \mathrm{d}t$ and $t_n + 2\mathrm{d}t$, respectively. $\mathrm{d}t$ denotes half the time step.

An SE associated with a point is the union of all planes containing the point. For example, $\mathrm{SE}(G')$ associated with point G', is the union of the hexagon $A'B'C'D'E'F'$, the quadrilaterals $B''BGG''$, $D''DGG''$, and $F''FGG''$. The surfaces of two neighbouring SEs form a spaced time cylinder which is a conservation element. For example, the surfaces of $\mathrm{SE}(G')$ $\mathrm{SE}(A)$, $\mathrm{SE}(C)$, and $\mathrm{SE}(E)$ form three CEs, which are the cylinders $ABGFA'B'G'F'$, $CDGBC'D'G'B'$, and $EFGDE'F'G'D'$ and they are referred to as $\mathrm{CE}_1(G')$, $\mathrm{CE}_2(G')$, and $\mathrm{CE}_3(G')$, respectively. $\mathrm{CE}(G')$ is the union of $\mathrm{CE}_1(G')$, $\mathrm{CE}_2(G')$, and $\mathrm{CE}_3(G')$.

At a solution point, for example $\bar{G}'$, the first-order Taylor series expansion is employed to discretize the flow variables and fluxes at point P inside $\mathrm{SE}(G')$.

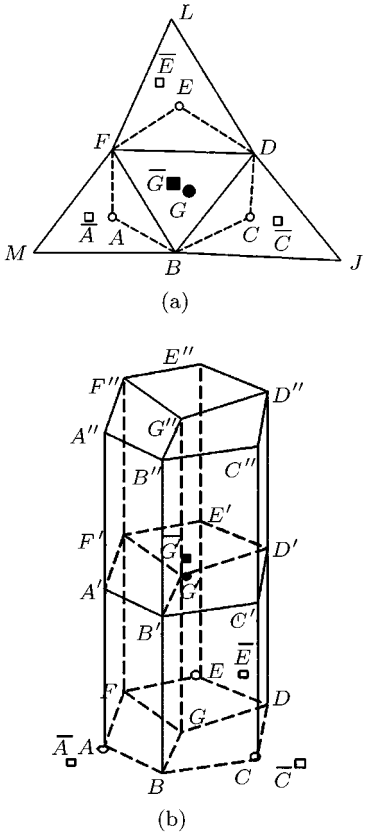


Fig. 1. Geometries of CE and SE: (a) the geometry of CE and SE in space, (b) CE(G') and SE(G').

Then Eq. (2) at CE(G') is approximated by variables and their derivatives at points $\bar{G}'$, $\bar{A}$, $\bar{C}$, and $\bar{E}$. Assume every two neighbouring CEs, for example $\mathrm{CE}_1(G')$, and $\mathrm{CE}_2(G')$, give a unique equation of $(U_m)_x$ and $(U_m)_y$. Then aided by Eq. (3), $(U_m)_x$ and $(U_m)_y$ at CE(G') can be yielded.

$$W(x_1,x_2,x_3)=\begin{cases}0, & \left(\prod_{i=1}^{3}\theta_i=0\right),\\ \dfrac{\sum_{i=1}^{3}x_i/|\theta_i|^{\alpha}}{\sum_{i=1}^{3}1/|\theta_i|^{\alpha}}, & \left(\prod_{i=1}^{3}\theta_i\neq 0\right),\end{cases} \tag{3}$$

where $\theta_i=\sqrt{((U_x)_i)^2+((U_y)_i)^2}$ and $\alpha\geq 1$.

The residual of CE(G') is obtained by adding all residuals of corresponding CEs ($\mathrm{CE}_1(G')$, $\mathrm{CE}_2(G')$, and $\mathrm{CE}_3(G')$). The residual of Chang's CE/SE scheme in $\mathrm{CE}_1(G')$ is obtained first. Then the residuals of $\mathrm{CE}_2(G')$ and $\mathrm{CE}_3(G')$ can be derived by replacing the points of $\mathrm{CE}_1(G')$ respectively.

For any points M and N with coordinates (x_M, y_M, t_M) and (x_N, y_N, t_N), let $\delta^x_{MN}=x_M-x_N$, $\delta^y_{MN}=y_M-y_N$, and $\delta^t_{MN}=t_M-t_N$, then, based on Taylor series expansion, the flow variables at point M can be approximated by variables at point N. Let $U_m(M;\ N)$ and $\Delta U_m(M;\ N)$ denote $U_m(N)+\delta^x_{MN}U_m(N)_x+\delta^y_{MN}U_m(N)_y+\delta^t_{MN}U_m(N)_t$ and $U_m(M)+\delta^t_{NM}U_m(M)_t-U_m(N)$, respectively.

Based on the second-order Taylor series expansion, the residual R_m at $\mathrm{CE}_1(G')$ is

$$\begin{aligned}S_{ABGF}R_m=\ & S_{ABGF}\{\mathrm{d}t[\big(U_m(\bar{G})_t+E_m(\bar{G})_x+F_m(\bar{G})_y\big)+\mathrm{d}t/2U_m(\bar{G})_{2t}+\delta^x_{A^*\bar{G}}U_m(\bar{G})_{xt}+\delta^y_{A^*\bar{G}}U_m(\bar{G})_{yt}]\\ &-[(2\delta^y_{A^*\bar{G}}-\delta^y_{\bar{A}\bar{G}})\delta^x_{\bar{A}\bar{G}}+(2\delta^x_{A^*\bar{G}}-\delta^x_{\bar{A}\bar{G}})\delta^y_{\bar{A}\bar{G}}]/2U_m(\bar{G})_{xy}-(2\delta^y_{A^*\bar{G}}-\delta^y_{\bar{A}\bar{G}})\delta^y_{\bar{A}\bar{G}}/2U_m(\bar{G})_{2y}\\ &-(2\delta^x_{A^*\bar{G}}-\delta^x_{\bar{A}\bar{G}})\delta^x_{\bar{A}\bar{G}}/2U_m(\bar{G})_{2x}\}+\mathrm{d}t/2\{(\delta^y_{B\bar{G}}-\delta^y_{\bar{A}F})\delta^y_{BF}[\delta^x_{\bar{A}\bar{G}}E_m(\bar{G})_{xy}+\delta^y_{\bar{A}\bar{G}}E_m(\bar{G})_{2y}]\\ &-(\delta^x_{B\bar{G}}-\delta^x_{\bar{A}F})\delta^x_{BF}[\delta^x_{\bar{A}\bar{G}}F_m(\bar{G})_{2x}+\delta^y_{\bar{A}\bar{G}}F_m(\bar{G})_{xy}]+\mathrm{d}t[(\delta^y_{BF}(\delta^x_{\bar{A}G}-\delta^x_{B\bar{G}})-\delta^y_{FG}\delta^x_{BF})E_m(\bar{G})_{xt}\\ &+(\delta^y_{BF}\delta^x_{FG}-(\delta^y_{\bar{A}G}-\delta^y_{B\bar{G}})\delta^x_{BF})F_m(\bar{G})_{yt}+\delta^y_{BF}(\delta^y_{\bar{A}F}-\delta^y_{B\bar{G}})E_m(\bar{G})_{yt}-\delta^x_{BF}(\delta^x_{\bar{A}F}-\delta^x_{B\bar{G}})F_m(\bar{G})_{xt}]\\ &+\delta^x_{\bar{A}\bar{G}}[(\delta^y_{BF}(\delta^x_{A\bar{G}}-\delta^x_{\bar{A}F})-\delta^y_{AB}\delta^x_{BF})E_m(\bar{G})_{2x}+(\delta^y_{BF}\delta^x_{AB}-(\delta^y_{A\bar{G}}-\delta^y_{\bar{A}F})\delta^x_{BF})F_m(\bar{G})_{xy}]\\ &+\delta^y_{\bar{A}\bar{G}}[(\delta^y_{BF}(\delta^x_{A\bar{G}}-\delta^x_{\bar{A}F})-\delta^y_{AB}\delta^x_{BF})E_m(\bar{G})_{xy}+(\delta^y_{BF}\delta^x_{AB}-(\delta^y_{A\bar{G}}-\delta^y_{\bar{A}F})\delta^x_{BF})F_m(\bar{G})_{2y}]\}.\end{aligned} \tag{4}$$

Applying Eq. (4) to $\mathrm{CE}_2(G')$ and $\mathrm{CE}_3(G')$, the residuals of flow variables in CE(G') are yielded. Only the coefficients of $E_m(\bar{G})_{2y}$ and $F_m(\bar{G})_{2x}$ in CE(G') are listed here. The two coefficients are

$$\mathrm{d}t\left(\delta^y_{\bar{A}\bar{C}}\left(\delta^y_{B\bar{G}}\right)^2+\delta^y_{\bar{C}\bar{E}}\left(\delta^y_{D\bar{G}}\right)^2+\delta^y_{\bar{E}\bar{A}}\left(\delta^y_{F\bar{G}}\right)^2+\delta^y_{BD}\left(\delta^y_{\bar{C}\bar{G}}\right)^2+\delta^y_{DF}\left(\delta^y_{\bar{E}\bar{G}}\right)^2+\delta^y_{FB}\left(\delta^y_{\bar{A}\bar{G}}\right)^2\right),$$

and

$$\mathrm{d}t\left(\delta^x_{\bar{C}\bar{A}}\left(\delta^x_{B\bar{G}}\right)^2+\delta^x_{\bar{E}\bar{C}}\left(\delta^x_{D\bar{G}}\right)^2+\delta^x_{\bar{A}\bar{E}}\left(\delta^x_{F\bar{G}}\right)^2+\delta^x_{DB}\left(\delta^x_{\bar{C}\bar{G}}\right)^2+\delta^x_{FD}\left(\delta^x_{\bar{E}\bar{G}}\right)^2+\delta^x_{BF}\left(\delta^x_{\bar{A}\bar{G}}\right)^2\right).$$

They are not equal to zero. Hence, Chang's CE/SE scheme is only first-order accurate for flow variables.

Referring to Eq. (4), in order to construct a second-order accurate scheme the following equations hold in $\mathrm{CE}_1(G')$:

$$\delta^y_{B\bar{G}}-\delta^y_{\bar{A}F}=0,\quad \delta^x_{B\bar{G}}-\delta^x_{\bar{A}F}=0,\quad \delta^y_{A^*\bar{G}}=\delta^y_{\bar{A}\bar{G}}/2,\quad \delta^x_{A^*\bar{G}}=\delta^x_{\bar{A}\bar{G}}/2. \tag{5}$$

Equation (5) implies that quadrilateral $\bar{A}B\bar{G}F$ is a parallelogram and A^* is the centroid of the line segment $\bar{A}\bar{G}$. As a result, all the similar quadrilaterals are parallelograms. This condition can be satisfied only for a structured mesh.

If a similar process is applied, the residuals of derivatives in the three CEs are derived as

$$
\begin{aligned}
R^1_{dm} &= \frac{\mathrm{d}t^2 U_m(\bar{G})_{2t} - \left(\delta^x_{\bar{A}\bar{G}}\right)^2 U_m(\bar{G})_{2x} - 2\delta^x_{\bar{A}\bar{G}}\delta^y_{\bar{A}\bar{G}} U_m(\bar{G})_{xy} - \left(\delta^y_{\bar{A}\bar{G}}\right)^2 U_m(\bar{G})_{2y}}{2},\\
R^2_{dm} &= \frac{\mathrm{d}t^2 U_m(\bar{G})_{2t} - \left(\delta^x_{\bar{C}\bar{G}}\right)^2 U_m(\bar{G})_{2x} - 2\delta^x_{\bar{C}\bar{G}}\delta^y_{\bar{C}\bar{G}} U_m(\bar{G})_{xy} - \left(\delta^y_{\bar{C}\bar{G}}\right)^2 U_m(\bar{G})_{2y}}{2},\\
R^3_{dm} &= \frac{\mathrm{d}t^2 U_m(\bar{G})_{2t} - \left(\delta^x_{\bar{E}\bar{G}}\right)^2 U_m(\bar{G})_{2x} - 2\delta^x_{\bar{E}\bar{G}}\delta^y_{\bar{E}\bar{G}} U_m(\bar{G})_{xy} - \left(\delta^y_{\bar{E}\bar{G}}\right)^2 U_m(\bar{G})_{2y}}{2},
\end{aligned}
\tag{6}
$$

where R^i_{dm} denotes the residuals of derivative terms in $\mathrm{CE}_i(G')$ $(i = 1, 2, 3)$. Based on Eq. (6), the derivatives are only first-order accurate. The same result is obtained for the other half time step.

According to the above discussion, the flow variables based on Chang's CE/SE scheme are second-order accurate for a 2D structured mesh and first-order accurate for a 2D unstructured mesh. The derivatives are first-order accurate for both types of mesh.

3. New CE/SE scheme

The redefinitions of SEs and CEs are proposed, in order to fix the inconvenience for unstructured grids. It makes use of both the centroids and the vertices of the triangles. All centroids of the triangles are located at the same time level and all vertices are at the neighbouring time levels. During the calculation, variables at the centroid are calculated based on vertices of the same triangle, and variables at the vertex are calculated based on the centroids of the triangles sharing the same vertex. By this means, the scheme no longer depends on the topology of the grid. The details are described below.

In Fig. 2(a), points A, B, C, D, E, and F are mesh nodes. Point A is the solution point of the polygon $O_1P_1O_2P_2O_3P_3O_4P_4O_5P_5$. Points P_1, P_2, P_3, P_4, and P_5, are the centroids of ΔAEF, ΔAFB, ΔABC, ΔACD, and ΔADE, respectively. They are also the solution points of the corresponding triangles. The two types of solution points are at different time levels. Points O_1, O_2, O_3, O_4, O_5, O_6, O_7, O_8, O_9, and O_{10} are the centroids of the line segment AE, AF, AB, AC, AD, AE, EF, FB, BC, CD, and DE, respectively. In the space–time domain as shown in Figs. 2(b) and 2(c), points without any superscript are at the time level t_n. Points with superscript $'$, $''$ and $'''$ are at the time level $t_n + \mathrm{d}t$, $t_n + 2\mathrm{d}t$ and $t_n - \mathrm{d}t$, respectively.

Based on the description of SE and CE in Section 2, $\mathrm{SE}(A')$ associated with point A' is the union of six planes, the polygon $O'_1P'_1O'_2P'_2O'_3P'_3O'_4P'_4O'_5P'_5$, the quadrilaterals $AA''O''_1O_1$, $AA''O''_2O_2$, $AA''O''_3O_3$, $AA''O''_4O_4$, and $AA''O''_5O_5$. Similarly, there are $\mathrm{SE}(A''')$, $\mathrm{SE}(E''')$, $\mathrm{SE}(F''')$, $\mathrm{SE}(P_1)$, $\mathrm{SE}(P_2)$, $\mathrm{SE}(P_3)$, $\mathrm{SE}(P_4)$, and $\mathrm{SE}(P_5)$ associated with A''', E''', F''', P_1, P_2, P_3, P_4, and P_5, respectively. $\mathrm{SE}(P_1)$, $\mathrm{SE}(P_2)$, $\mathrm{SE}(P_3)$, $\mathrm{SE}(P_4)$, and $\mathrm{SE}(P_5)$ form five CEs between time level t_n and $t_n + \mathrm{d}t$. They are cylinders $O'_1P'_1O'_2A'O_1P_1O_2A$, $O'_2P'_2O'_3A'O_2P_2O_3A$, $O'_3P'_3O'_4A'O_3P_3O_4A$, $O'_4P'_4O'_5A'O_4P_4O_5A$, and $O'_5P'_5O'_1A'O_5P_5O_1A$, and they are referred to as $\mathrm{CE}_1(A')$, $\mathrm{CE}_2(A')$, $\mathrm{CE}_3(A')$, $\mathrm{CE}_4(A')$, and $\mathrm{CE}_5(A')$, respectively. $\mathrm{CE}(A')$ is the union of the five CEs. $\mathrm{SE}(A''')$, $\mathrm{SE}(E''')$, $\mathrm{SE}(F''')$, and $\mathrm{SE}(P_1)$ form three CEs between time level $t_n - \mathrm{d}t$ and t_n. The three CEs are cylinders $O'''_1P'''_1O'''_2A'''O_1P_1O_2A$, $O'''_6P'''_1O'''_1E'''O_6P_1O_1E$, and $O'''_2P'''_1O'''_6F'''O_2P_1O_6F$, and they are referred to as $\mathrm{CE}_1(P_1)$, $\mathrm{CE}_2(P_1)$, and $\mathrm{CE}_3(P_1)$, respectively. $\mathrm{CE}(P_1)$ is the union of the three CEs.

The new CE/SE scheme has a similar procedure of solving the flow variables to Chang's scheme. For example, $U_m(P_1)$ are yielded as

$$
\begin{aligned}
U_m(P_1)S_{AEF} = {} & S_{AO_1P_1O_2}U_m(A^*;A''') + S_{EO_6P_1O_1}U_m(E^*;E''') + S_{FO_2P_1O_6}U_m(F^*;F''')\\
& - \mathrm{d}t[\delta^y_{AO_1}E_m(C_{O_1'''O_1AA'''};A''') - \delta^x_{AO_1}F_m(C_{O_1'''O_1AA'''};A''') + \delta^y_{O_1E}E_m(C_{E'''EO_1O_1'''};E''')\\
& - \delta^x_{O_1E}F_m(C_{E'''EO_1O_1'''};E''') + \delta^y_{EO_6}E_m(C_{O_6'''O_6EE'''};E''') - \delta^x_{EO_6}F_m(C_{O_6'''O_6EE'''};E''')\\
& + \delta^y_{O_6F}E_m(C_{F'''FO_6O_6'''};F''') - \delta^x_{O_6F}F_m(C_{F'''FO_6O_6'''};F''') + \delta^y_{FO_2}E_m(C_{O_2'''O_2FF'''};F''')
\end{aligned}
$$

$$- \delta^x_{FO_2} F_m(C_{O_2'''O_2FF'''}; F''') + \delta^y_{O_2A} E_m(C_{A'''AO_2O_2'''}; A''') - \delta^x_{O_2A} F_m(C_{A'''AO_2O_2'''}; A''')], \quad (7)$$

where S_{AEF}, $S_{AO_1P_1O_2}$, $S_{EO_6P_1O_1}$, and $S_{FO_2P_1O_6}$ denote the areas of the triangle AEF, the quadrilaterals $AO_1P_1O_2$, $EO_6P_1O_1$, and $FO_2P_1O_6$, respectively; A^*, E^*, and F^* denote the centroids of the quadrilateral $AO_1P_1O_2$, $EO_6P_1O_1$, and $FO_2P_1O_6$, respectively.

To calculate $(U_m)_x$ and $(U_m)_y$, the function $W(x_1, x_2, x_3)$ is expanded as

$$W(x_1, x_2, \ldots, x_n) = \begin{cases} 0, & \left(\prod_{i=1}^n \theta_i = 0\right), \\ \dfrac{\sum_{i=1}^n x_i / |\theta_i|^\alpha}{\sum_{i=1}^n 1 / |\theta_i|^\alpha}, & \left(\prod_{i=1}^n \theta_i \neq 0\right), \end{cases} \quad (8)$$

where $\theta_i = \sqrt{((U_x)_i)^2 + ((U_y)_i)^2}$, $\alpha \geq 1$, and $n \geq 2$.

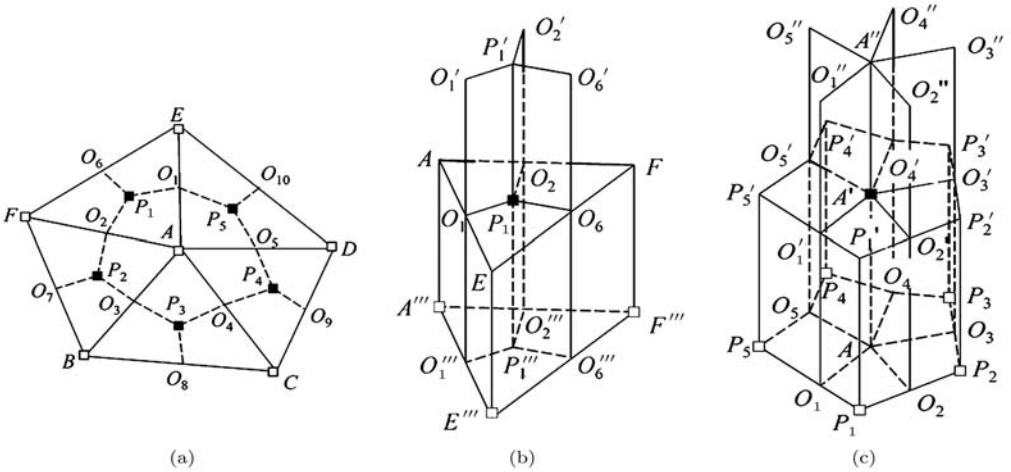


Fig. 2. Geometries of CE and SE in space and time with mesh points A, B, C, D, E, F, and time step $\mathrm{d}t$: (a) and CE and SE in space; (b) CE(P_1) and SE(P_1); and (c) CE(A') and SE(A').

The equations of $(U_m)_x$ and $(U_m)_y$ between two neighbouring CEs are yielded next. Take $\mathrm{CE}_1(P_1)$ and $\mathrm{CE}_2(P_1)$ for example. Based on the Taylor series expansion, flow variables at point A can be approximated by P_1 or A'''. Assume that they give the same value at point A. Equation (9) is obtained as

$$\delta^x_{AP_1} U_m(P_1)_x + \delta^y_{AP_1} U_m(P_1)_y = U_m(A''') + \mathrm{d}t U_m(A''')_t - U_m(P_1). \quad (9)$$

Similarly, equation (10) is obtained as

$$\delta^x_{EP_1} U_m(P_1)_x + \delta^y_{EP_1} U_m(P_1)_y = U_m(E''') + \mathrm{d}t U_m(E''')_t - U_m(P_1). \quad (10)$$

By solving Eqs. (9) and (10), the expressions of $U_m(P_1)_x|_{O_1}$ and $U_m(P_1)_y|_{O_1}$ are obtained. $U_m(P_1)_x|_{O_1}$ and $U_m(P_1)_y|_{O_1}$ denote $U_m(P_1)_x$ and $U_m(P_1)_y$ between $\mathrm{CE}_1(P_1)$ and $\mathrm{CE}_2(P_1)$, respectively. The line segment P_1O_1 is shared by two CEs. Similar symbols in Eq. (11) have similar meanings. For example, $U_m(P_1)_x|_{O_2}$ denotes $U_m(P_1)_x$ between two neighbouring CEs, which share the line segment P_1O_2.

Finally, $(U_m)_x$ and $(U_m)_y$ at the solution point are derived by adding up all the corresponding values. For example,

$$\begin{aligned} U_m(P_1)_x &= W\left(U_m(P_1)_x|_{O_1}, U_m(P_1)_x|_{O_2}, U_m(P_1)_x|_{O_6}\right), \\ U_m(P_1)_y &= W\left(U_m(P_1)_y|_{O_1}, U_m(P_1)_y|_{O_2}, U_m(P_1)_y|_{O_6}\right). \end{aligned} \quad (11)$$

Based on $W(x_1, x_2, \ldots, x_n)$, it is hard to analyse the CE/SE scheme with α. Moreover, the dissipation, introduced by α, is below the average value of all variables and above the value of the minmod function. Hence, a new parameter β is proposed to increase the range of the dissipation and to simplify the process of analysing the CE/SE scheme.

According to Green's theorem, the second-order derivatives inside a domain S can be approximated by

$$
\begin{aligned}
&(U_{2x})\,|_S \approx \frac{1}{S}\int \frac{\partial^2 U}{\partial x^2}\,\mathrm{d}S = \frac{1}{S}\oint_{\partial S}\frac{\partial U}{\partial x}n_x\,\mathrm{d}l,\ (U_{2y})\,|_S \approx \frac{1}{S}\int \frac{\partial^2 U}{\partial y^2}\,\mathrm{d}S = \frac{1}{S}\oint_{\partial S}\frac{\partial U}{\partial y}n_y\,\mathrm{d}l,\\
&(U_{xy})\,|_S \approx \frac{1}{S}\int \frac{\partial^2 U}{\partial x\partial y}\,\mathrm{d}S = \frac{1}{2S}\oint_{\partial S}\left(\frac{\partial U}{\partial y}n_x + \frac{\partial U}{\partial x}n_y\right)\mathrm{d}l,\\
&(U_{2t})\,|_S = -\left(\frac{\partial^2 E}{\partial x\partial t} + \frac{\partial^2 F}{\partial y\partial t}\right)|_S \approx \frac{-1}{S}\oint_{\partial S}\left(\frac{\partial E}{\partial t}n_x + \frac{\partial F}{\partial t}n_y\right)\mathrm{d}l,
\end{aligned}
\tag{12}
$$

where $(U_{2x})\,|_S$, $(U_{2y})\,|_S$, $(U_{xy})\,|_S$, and $(U_{2t})\,|_S$ denote $\partial^2U/\partial x^2$, $\partial^2U/\partial y^2$, $\partial^2U/\partial x\partial y$, and $\partial^2U/\partial t^2$ inside S, respectively.

Aided by Eq. (12), equation (6) is second-order accurate if equation (13) is added to it.

$$
\begin{cases}
-\dfrac{\mathrm{d}t^2(U_m)_{2t}\,|_{S(G)} - \left(\delta^x_{\bar{A}\bar{G}}\right)^2(U_m)_{2x}\,|_{S(G)} - 2\delta^x_{\bar{A}\bar{G}}\delta^y_{\bar{A}\bar{G}}(U_m)_{xy}\,|_{S(G)} - \left(\delta^y_{\bar{A}\bar{G}}\right)^2(U_m)_{2y}\,|_{S(G)}}{2},\\
-\dfrac{\mathrm{d}t^2(U_m)_{2t}\,|_{S(G)} - \left(\delta^x_{\bar{C}\bar{G}}\right)^2(U_m)_{2x}\,|_{S(G)} - 2\delta^x_{\bar{C}\bar{G}}\delta^y_{\bar{C}\bar{G}}(U_m)_{xy}\,|_{S(G)} - \left(\delta^y_{\bar{C}\bar{G}}\right)^2(U_m)_{2y}\,|_{S(G)}}{2},\\
-\dfrac{\mathrm{d}t^2(U_m)_{2t}\,|_{S(G)} - \left(\delta^x_{\bar{E}\bar{G}}\right)^2(U_m)_{2x}\,|_{S(G)} - 2\delta^x_{\bar{E}\bar{G}}\delta^y_{\bar{E}\bar{G}}(U_m)_{xy}\,|_{S(G)} - \left(\delta^y_{\bar{E}\bar{G}}\right)^2(U_m)_{2y}\,|_{S(G)}}{2},
\end{cases}
\tag{13}
$$

where $S(G)$ denotes the computational domain $ABCDEF$. To adjust the oscillation of the new scheme, each term of equation (13) is multiplied by the new parameter β ($-\infty \le \beta \le 1$). If $\beta = 1$, the derivatives are second-order accurate. As β is smaller, the numerical oscillation is weaker. Furthermore, unlike α, the expense of changing the dissipation is nearly independent of the value of β. Let $\alpha = 0$, the analysis of the CE/SE scheme is simplified and the appropriate value of β can be achieved.

4. Examples and discussion

In this section, we examine the accuracy and the efficiency of the new CE/SE scheme. The grid used by the new CE/SE scheme in the first example is constructed by splitting each rectangle into two triangles. The second example validates the performance of the new CE/SE scheme on unstructured grids. In order to compare it with Wang's CE/SE scheme, the new CE/SE scheme with $\alpha = 1$ is selected for all examples. As discussed in Section 3, β is difficult to obtain. Hence, only the range of β is discussed below.

4.1. The shock reflection problem

The shock reflection problem, which is a standard test case for a 2D scheme is introduced to test the new scheme thoroughly. The computational domain is 4.0×1.0 and the size of the rectangular cell is 0.01×0.01.

Figure 3 shows the pressure contour at $y = 0.5$ with $t = 2.5$ for different schemes, which are the 5th WENO scheme, Wang's CE/SE scheme[10] and the new CE/SE scheme with different values of β. In Fig. 3, WENO35, new CE/SE $\beta = 0$, new CE/SE $\beta = 1$, new CE/SE $\beta = 0.5$, new CE/SE $\beta = 0.4$, new CE/SE $\beta = 0.3$, and new CE/SE $\beta = -0.5$ denote the fifth-order accurate WENO scheme, the new CE/SE schemes with $\beta = 0$, 1, 0.5, 0.4, 0.3, and –0.5, respectively. Referring to Figs. 3(a) and 3(b), all solutions approach the numerical result obtained with the WENO35 scheme. A small oscillation near the shock wave, which is obtained with the new CE/SE scheme with $\beta = 1$, is observed. While the solution of the new CE/SE scheme with $\beta = 0$ shows overly strong dissipation. As discussed in Section 3, larger β introduces stronger oscillation. In the case of $\beta = 1$, the introduced oscillation is too strong to be canceled by the numerical dissipation. In the case of $\beta = 0$, the introduced oscillation is not enough to cancel the excessive numerical dissipation. Thus the reasonable β is between 0 and 1. To give the reasonable value of β, the pressure contour obtained by the new CE/SE schemes respectively with $\beta = 1.0$, 0.5, 0.4, 0.3, 0, and –0.5 are illustrated in Figs. 3(c) and 3(d). During the simulation, the Courant number is the same for all values of β. The numerical results indicate that the reasonable range of β is [0, 0.5]. Although $\beta = 0.5$ gives nearly the same solution as that of the WENO35 scheme, the value 0.3 is suggested for its stronger dissipation and better steadiness.

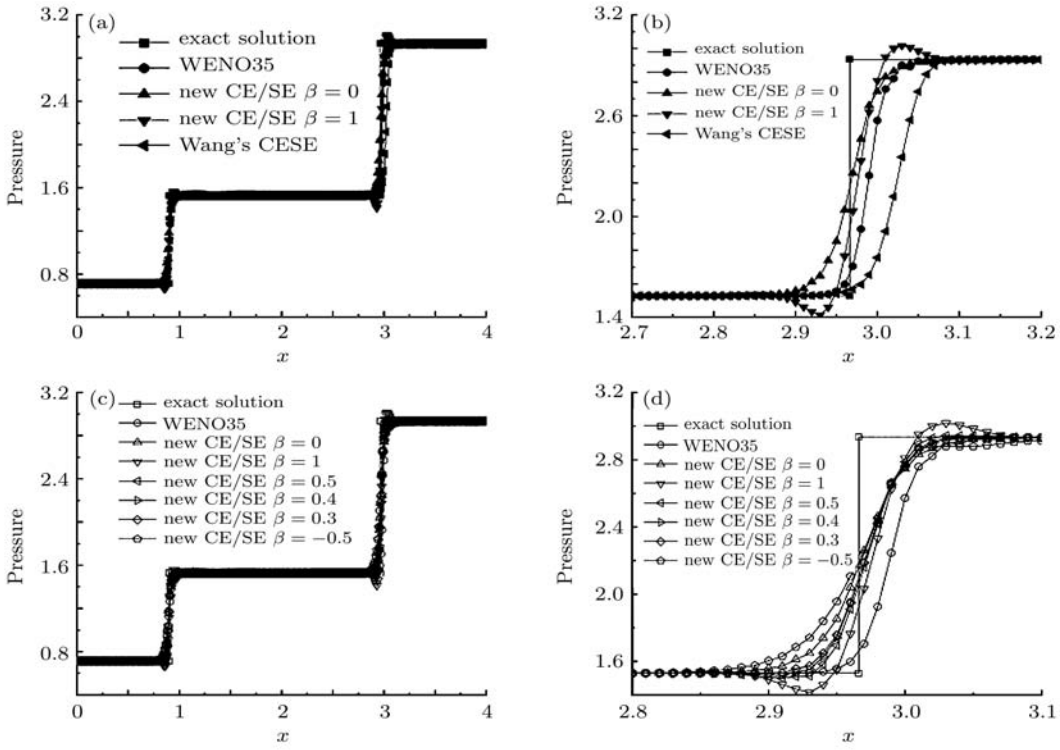


Fig. 3. Distributions of pressure calculated by different schemes for the oblique shock problem at $y = 0.5$: (a) the distribution of pressure for different schemes, (b) the magnification of the reflected shock, (c) the distributions of pressure for different values of β, (d) the magnification of the reflected shock.

The computational time denoted by CPU time is also listed in Table 1 to discuss the efficiency of the new CE/SE scheme due to different values of β or α. Refer to Table 1. The change of β leads to less than 1.5% change of CPU time while the change of α leads to over 50% change. This proves that the expense of changing the dissipation is nearly independent of the value of β. Table 1 also implies that the efficiency of the new CE/SE scheme with $\alpha = 1$ is about twice that of the WENO35 scheme due to its lack of flux splitting process and the third-order accurate RK method.

Table 1. The CPU time spent by different methods with the same time step.

	WENO35	New CE/SE α=1			New CE/SE β=0		
		$\beta = 0$	$\beta = 0.2$	$\beta = 1$	$\alpha = 0$	$\alpha = 0.2$	$\alpha = 1$
CPU time/s	3132.047	1590.67	1576.81	1596.91	931.563	2543.17	1590.67
Relative time	1	0.508	0.503	0.510	0.297	0.812	0.508

4.2. Supersonic flow passing over a circular cylinder

This case is introduced to test the behaviour of the new CE/SE scheme at unstructured grids. The initial condition is $(\rho_0,\ u_0,\ v_0,\ p_0) = (1.4, Ma, 0, 1)$, where ρ_0, u_0, v_0, p_0, and Ma denote the density, the x component of velocity, the y component of velocity, the pressure, and the Mach number at the time of $t = 0$, respectively. The Mach numbers are 2, 2.7, 3, 3.5, and 4, respectively. The height of the grid cell near the shock is roughly equal to 1/25. In order to reduce the influence of the low accuracy near the boundary, the height of the grid cell near the cylinder is equal to 1/50. The simulation is calculated till t reaches 10.0.

To obtain an appropriated value of β, β is taken as 0, 0.1, and 0.2 for the case of $Ma = 3$. The contour of pressure is illustrated in Fig. 4. Referring to Fig. 4, all three values of β give indistinguishable results. Hence, the evolution of the numerical error is plotted in Fig. 5. As shown in Fig. 5, the quickest convergence speed and the highest accuracy are observed for $\beta = 0.2$. Therefore, β is taken as 0.2 for the remaining cases.

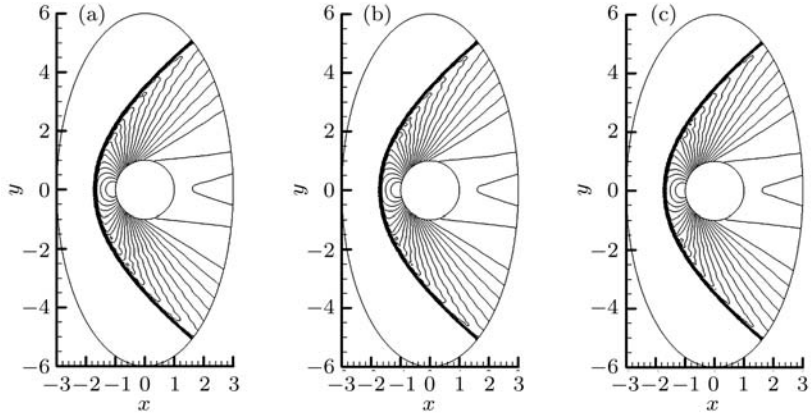


Fig. 4. Distributions of pressure for $Ma = 3.0$, calculated with the new unstructured CE/SE scheme for $\beta = 0$ (a), 0.1 (b), and 0.2 (c).

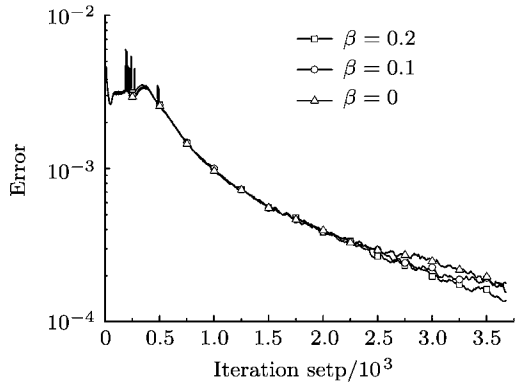


Fig. 5. Errors of the new CE/SE scheme for different values of β.

As is well known, as the Mach number increases, the shock wave approaches the cylinder causing the maximum value of the coefficient of pressure (Cp) to reach 2.0 and the minimum value of Cp to increase. Figure 6 shows the distance between the shock and the cylinder which is obtained experimentally[23] and numerically by the third-order accurate ENO scheme and the new CE/SE scheme. In Fig. 6, D is the diameter of the cylinder and d is the distance between the shocks at $y = 0$ and $(-1, 0)$. As shown in Fig. 6, both schemes obtain satisfactory results and predict the right trend. The new CE/SE scheme gives less than 5% error for $Ma = 2$ and 2.7 and about half of the error obtained by ENO scheme for $Ma = 4$. It indicates that the new CE/SE scheme with $\beta = 0.2$ is less dissipative and more accurate than ENO scheme. Curves for theta-dependent pressure coefficient Cp on the cylinder in the polar coordinate system are also plotted for $Ma = 2$, 3 and 4 in Fig. 7, where θ denotes polar angle. As shown in Fig. 7, the new CE/SE scheme predicts the right trend. However, the distribution of Cp is not satisfactory because of the oscillation caused by the boundary condition. Hence, finding a more robust and accurate technique of calculating the boundary condition is one of our following works.

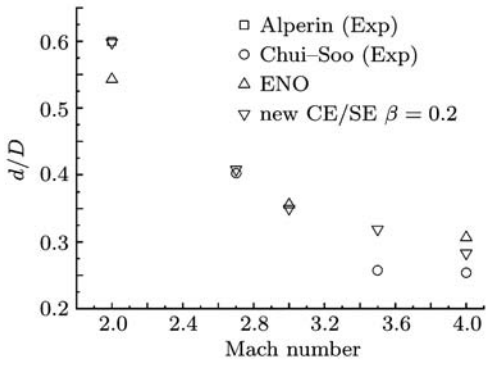


Fig. 6. Distances between the shock at $y = 0$ and the point $(-1, 0)$ for different Mach numbers.

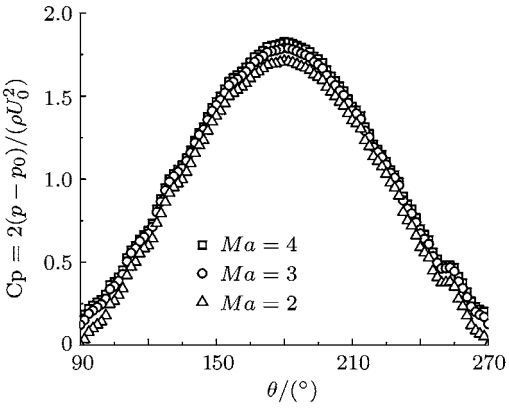


Fig. 7. Theta-dependent coefficient of pressure Cp on the cylinder for different Mach numbers.

From both examples, we conclude that the new CE/SE scheme with an appropriated β value is more capable of capturing weak shock waves than the fifth-order accurate WENO scheme. The reason is that the two methods have different objectives. The WENO

scheme focuses on eliminating oscillation causing excessive dissipation near weak shock waves. While the new CE/SE scheme concentrates on achieving high resolution, leading to oscillation near strong shock waves. In this paper, all shock waves are weak. Thus the new CE/SE scheme performs better than the fifth-order accurate WENO scheme.

5. Conclusion

The accuracy of Chang's unstructured CE/SE method is theoretically investigated. The result reveals that the unstructured CE/SE method is less accurate than the structured CE/SE method. Moreover, redefinitions of CE and SE, which can directly extend CE/SE schemes to any type of grid cell, are proposed. An extra parameter β is also introduced to improve the accuracy and the efficiency. Compared with Chang's original parameter, β does not require extra computational resources when it is increased. Numerical tests indicate that the new CE/SE scheme with an appropriate β is better at capturing shock waves than Wang's CE/SE scheme and it is even better than the ENO/WENO scheme.

The new CE/SE scheme has extended the application of the CE/SE scheme. It provides engineers with a powerful tool for simulating shock waves.

References

[1] Yee H C, Warming R F and Harten A 1985 *J. Comput. Phys.* **57** 327

[2] Harten A, Osher S, Engquist B and Chakravarthy S R 1986 *Appl. Numer. Math.* **2** 347

[3] Xuan L J and Wu J Z 2010 *J. Comput. Phys.* **229** 5999

[4] Shu C W 1997 *NASA* CR-97-206253

[5] Chang S C 1995 *J. Comput. Phys.* **119** 295

[6] Chang S C 2010 *AIAA* 2010-543

[7] Li X and Weng C S 2009 *Chin. Sci. Bull.* **54** 1641

[8] Ji Z and Zhou Y F 2010 *Chin. Phys. Lett.* **27** 085201

[9] Wang G, Wang J T and Liu K X 2010 *Sci. Chin.* Ser. G: *Phys. Mech. Astron.* **53** 237

[10] Wang G, Zhang D L and Liu K X 2007 *Chin. Phys. Lett.* **24** 3563

[11] Wang G, Zhang D L and Liu K X 2010 *Chin. Phys. Lett.* **27** 024701

[12] Wang G, Zhang D L, Liu K X and Wang J T 2010 *Comput. Fluids* **39** 168

[13] Wang G, et al. 2011 *Comput. Phys. Commun.* **182** 1589

[14] Dong, H F, Hong T and Zhang D L 2011 *Chin. Phys. Lett.* **28** 030203

[15] Weng C S and Gore J P 2005 *Acta Mech. Sin.* **21** 32

[16] Chen Q Y, Wang J T and Liu K X 2010 *J. Comput. Phys.* **229** 7503

[17] Zhang Z C and Yu S T 2001 *AIAA* 2001-2592

[18] Chang C L 2006 *AIAA* 2006-4780

[19] Venkatachari B S, Cheng G C and Chang S C 2005 *AIAA* 2005-00931

[20] Liu K X and Wang J T 2004 *Chin. Phys. Lett.* **21** 2085

[21] Wang J T, Liu K X and Zhang D L 2009 *Comput. Fluids* **38** 544

[22] Wang X Y and Chang S C 1999 *CFD Journal* **8** 309

[23] Hui Q Q and Wang J P 2004 *Acta Aerodyn. Sin.* **22** 73 (in Chinese)